

Scientific paper

QSAR Studies and Structure Property/Activity Relationships Applied in Pyrazine Derivatives as Antiproliferative Agents Against the BGC823

Fatima Soualmia,^{1,2} Salah Belaidi,^{2,*} Nouredine Tchouar,¹ Touhami Lanez³
and Samia Boudergua^{1,4}

¹ Laboratoire Génie des Procédés et Environnement (GPE), Faculté de chimie, Université des sciences et technologies d'Oran (USTO) BP 1503 Oran 31000, Algérie

² University of Biskra, Group of Computational and Medicinal Chemistry, LMCE Laboratory, BP 145 Biskra 07000, Algeria

³ University of El-Oued, Faculty of Sciences and Technology, VTRS Laboratory, B.P.789, 39000, El-Oued, Algeria

⁴ University of KhemisMiliana, Faculty of Sciences and Technology, 44225, Ain Defla, Algeria

* Corresponding author: E-mail: s.belaidi@univ-biskra.dz.

Received: 04-08-2021

Abstract

Electronic structures, the effect of the substitution, structure physicochemical property/activity relationships and drug-likeness applied in pyrazine derivatives, have been studied at *ab initio* (HF, MP2) and B3LYP/DFT (density functional theory) levels. In the paper, the calculated values, i.e., NBO (natural bond orbitals) charges, bond lengths, dipole moments, electron affinities, heats of formation and quantitative structure-activity relationships (QSAR) properties are presented. For the QSAR studies, we used multiple linear regression (MLR) and artificial neural network (ANN) statistical modeling. The results show a high correlation between experimental and predicted activity values, indicating the validation and the good quality of the derived QSAR models. In addition, statistical analysis reveals that the ANN technique with (9-4-1) architecture is more significant than the MLR model. The virtual screening based on the molecular similarity method and applicability domain of QSAR allowed the discovery of novel anti-proliferative activity candidates with improved activity.

Keywords: Pyrazine; DFT; QSAR; MLR; ANN.

1. Introduction

Pyrazine is a heterocyclic compound containing two nitrogen atoms in its aromatic ring with molecular formula $C_4H_4N_2$.¹ It is a symmetrical molecule with point group D_{2h} .

Pyrazine is less basic than pyridine, pyridazine and pyrimidine. Tetramethyl pyrazine (also known as ligustrazine) is reported to scavenge superoxide anion and decrease nitric oxide production in human polymorph nuclear leukocytes and is a component of some herbs in traditional Chinese medicine. Some pyrazine derivatives contain various pharmacological effects: anti-cancer, anti-depressant and anxiolytic, tuberculosis, an anti-diabetic drug and pulmonary hypertension and cardiac valve.²⁻⁷

Quantum chemistry methods play an important role in obtaining molecular structures and predicting various

properties. To obtain highly accurate geometries and physical properties for molecules that are built from electronegative elements, expensive *Ab initio*/MP2 electron correlation methods are required.⁸ Density functional theory methods⁹⁻¹⁴ offer an alternative use of inexpensive computational methods which could handle relatively large molecules.¹⁵⁻²⁰

Quantitative structure-activity relationships (QSAR)²¹⁻²⁵ are attempts to correlate molecular structure, or properties derived from molecular structure, with a particular kind of chemical or biochemical activity. The kind of activity is a function of the interest of the user. QSAR is widely used in pharmaceutical, environmental and agricultural chemistry in the search for particular properties. The molecular properties used in the correla-

tions relate as directly as possible to the key physical or chemical processes taking place in the target activity.²⁶

This work is planned to illuminate the theoretical determination of the optimized molecular geometries, MESP, NBO charges of pyrazine compounds. In addition, we calculated important quantities such as the HOMO–LUMO energy gap.²⁷

Lipinski's 'Rule of Five'²⁸ as well as other parameters is useful a tools to aid in choosing oral drug candidates. Drug-likeness is described to encode the balance among the molecular properties of a compound that influences its pharmacodynamics, pharmacokinetics and ADME (absorption, distribution, metabolism and excretion) in a human body like a drug.²⁹

These parameters allow estimating oral absorption or membrane permeability, which occurs when evaluated molecules obey Lipinski's rule-of-five. Other parameters that are included the number of rotatable bonds, molecular volume, molecular polar surface area and the in vitro plasma protein binding.

The present paper deals with a specific organizational form of molecular matter. Other forms are given for example in the References.^{30–34}

Many different chemometric methods, such as multiple linear regression (MLR),³⁵ partial least squares regression (PLS),³⁶ different types of artificial neural networks (ANN),^{37–40} genetic algorithms (GA)⁴¹ and support vector machine (SVM) can be employed to deduce correlation models between the molecular structure and properties. At present, we derive a quantitative structure-activity relationship (QSAR) model using multiple linear regression (MLR) as well as artificial neural network (ANN) methods for the series of pyrazine derivatives.

The goal of the present study is to validate a suitable methodology for the accurate prediction of molecular geometries and energetic properties of potentially active compounds, and to determine the best molecular descriptors to be used in conjunction with linear (MLR) and non-linear (ANN) QSAR models to identify the best candidates for antiproliferative agents against the BGC823. The obtained QSAR models were finally employed to identify biological activities of potentially novel active compounds using in silico screening procedures.

2. Materials and Methods

All calculations were performed using HyperChem 8.0.6 software⁴² and Gaussian 09 program package⁴³, Marvin Sketch 6.2.1 software⁴⁴, Molinspiration online database⁴⁵ and JMP 8.0.2 software.⁴⁶

The geometries of pyrazine and their methyl, ethyl, bromo, fluoro derivatives were fully optimized with *ab initio*/HF, MP2 and DFT/B3LYP methods, using both basis set 6-311G ++(d,p) and cc-pVDZ integrated with Gaussian 09 program package. The calculation of QSAR proper-

ties is performed through the module QSAR properties (HyperChem version 8.0.6), which allows several properties commonly used in QSAR studies to be calculated.

Molinspiration, web-based software was used to obtain parameters such as TPSA (topological polar surface area), nrotb (number of rotatable bonds) and drug-likeness.

Multiple Linear Regression MLR analysis and artificial neural networks ANN were carried out using the software JMP 8.0.2.

The calculated results have been reported in the present work.

3. Results and Discussion

3.1. Geometric and Electronic Structure of Pyrazine

The optimized geometrical parameters of pyrazine with *ab initio*/HF, *ab initio*/MP2 and DFT method using 6-311G ++ (d, p) and cc-pVDZ basis set. Results concerning bond length values for pyrazine are listed in (Table 1), bond angles are listed in (Table 2) with the experimental results⁴⁷ and charge densities are listed in (Table 3) are following the numbering scheme given in (Fig. 1).

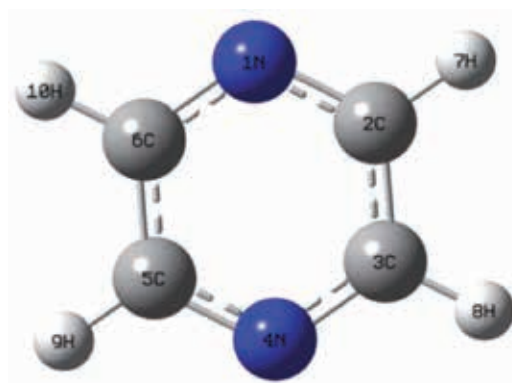


Fig. 1. 3D conformation of pyrazine (GaussView 5.0.8).

The efficiency of the DFT/B3LYP method with cc-pVDZ basis set may be scrutinized by comparison with the results obtained by more elaborate calculations such as *ab initio*/HF and MP2 methods. A very good agreement between predicted geometries (bond lengths and bond angles) and corresponding experimental data was obtained especially through the DFT/B3LYP results.

From that, we can say that the DFT method is more appropriate for further study on the pyrazine rings. Charge densities calculated by DFT/B3LYP are almost similar to *ab initio*/HF and MP2 methods. The geometry of the pyrazine is symmetric and planar; as all the dihedral angles are either nearly 0° or 180°, which makes this conforma-

tion more stable. The total atomic charges of pyrazine obtained from NBO charges with DFT/B3LYP and *ab initio*/HF and MP2 methods with cc-pVDZ basis set are listed in Table 3. The atoms N have negative charges which lead to an electrophilic attack, the atoms C and H have a positive charges which leads to the preferential site to nucleophilic attack.

The molecular electrostatic potential surface (MESP) is a plot of electrostatic potential mapped on to the constant electron density surface. In the majority of the MESP the maximum negative region which preferred the site for an electrophilic attack is indicated in red color, while the maximum positive region which preferred the site for a nucleophilic attack is symptoms indicated in blue color.⁴⁸ MESP has been found to be a very useful tool in the investigation of the correlation between the molecular structure and the physicochemical property relationship of molecules including biomolecules and drugs.^{49–53}

The MESP surface and contour map of pyrazine (Fig. 2) show the three regions characterized by red color (negative electrostatic potential) around the two cyclic nitrogen atoms which explain the ability of an electrophilic at-

tack on these positions, also the blue color (positive electrostatic potential) around the four hydrogen atoms which explain that these regions are susceptible for a nucleophilic attack. The green color situated in the middle between the red and blue regions explains the neutral electrostatic potential surface.

Table 3. NBO charges of pyrazine molecule.

Pyrazine Atoms	DFT/B3LYP cc-pVDZ	Ab initio/HF cc-pVDZ	Ab initio/MP2 cc-pVDZ
C	0.013	0.044	0.033
N	-0.456	-0.492	-0.487
H	0.215	0.202	0.210

3. 2. Substitution Effect on Pyrazine Structure

Calculated values of the two studied series indicated that in the first series methyl and ethyl groups with effects of electron donors, however, in the second series bromo and fluoro groups with effects of electron acceptors in po-

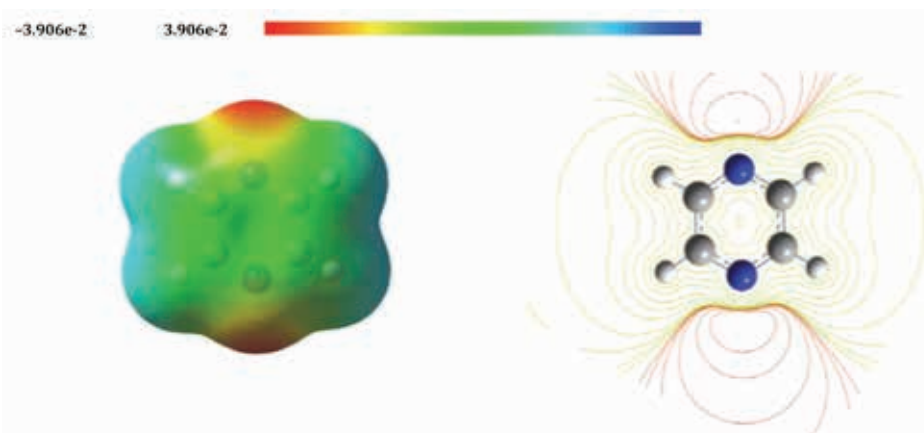


Fig. 2. 3D MESP surface map and 2D MESP contour map for pyrazine (Gauss view 5).

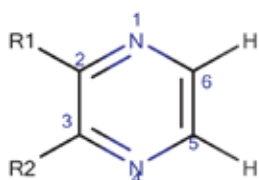
Table 1. Calculated bond lengths (angstrom) of pyrazine molecule.

Distance	EXP ⁴⁷	DFT/B3LYP		Ab initio/HF		Ab initio/MP2	
		6-311G ++ (d, p)	cc-pVDZ	6-311G ++ (d, p)	cc-pVDZ	6-311G ++ (d, p)	cc-pVDZ
C-N	1.338	1.335	1.339	1.317	1.320	1.343	1.349
C-C	1.397	1.394	1.398	1.386	1.388	1.399	1.405
C-H	1.083	1.086	1.095	1.075	1.082	1.087	1.096

Table 2. Angles in degree of pyrazine molecule.

Angle	EXP ⁴⁷	DFT/B3LYP		Ab initio/HF		Ab initio/MP2	
		6-311G++(d, p)	cc-PVDZ	6-311G++ (d, p)	cc-pVDZ	6-311G++(d, p)	cc-pVDZ
CCH	120.0	120.0	120.8	120.8	120.8	120.7	120.6
CNC	115.7	116.1	115.6	116.6	116.3	115.2	114.6

sitions C2 and C3 in the same series are given in (Table 4) and (Table 5), the heat of formation, dipole moment (μ) and HOMO (Highest Occupied Molecular Orbital) and LUMO (Lowest Unoccupied Molecular Orbital) energies of pyrazine systems are presented in (Fig. 3), NBO charges of pyrazine derivatives are reported in (Table 6) for the first series and in (Table 7) for the second series. This calculation is performed with DFT/B3LYP method using the cc-pVDZ basis set.

**Series 1**

- (A1) R1 = H, R2 = H
 (A2) R1 = CH₃, R2 = H
 (A3) R1 = CH₃, R2 = CH₃
 (A4) R1 = C₂H₅, R2 = H
 (A5) R1 = C₂H₅, R2 = C₂H₅

Series 2

- (B1) R1 = H, R2 = H
 (B2) R1 = Br, R2 = H
 (B3) R1 = Br, R2 = Br
 (B4) R1 = F, R2 = H
 (B5) R1 = F, R2 = F

Fig. 3. Structure of pyrazine derivatives (Marvin sketch15.8.31).

For each addition of methyl, ethyl and fluoro, the heat of formation decreases approximately 6, 12 or 39 (kcal · mol⁻¹) respectively but the addition of the bromo group leads to the increase of the heat of formation with 6 (kcal · mol⁻¹) approximately.

The Frontier orbitals, the highest occupied molecular orbital (HOMO) and lowest unoccupied molecular orbital (LUMO) are important factors in quantum chemistry⁵⁴ as these determine the way the molecule interacts with other species. The frontier reactivity and kinetic stability of the molecule. A molecule with a small frontier orbital gap

is more polarizable and is generally associated with a high chemical reactivity, low kinetic stability and is also termed a soft molecule.⁵⁵

For the first series, it was found that electron donors of compound A4 (2-ethyl pyrazine) has the lowest energy gap HOMO-LUMO (0.1958) and compound B3 (2,3-dibromopyrazine) has the lowest energy gap (0.1927) for the second series (Fig. 4).

From HSAB (Hard Soft Acid and Base) principle the lowest energetic gap allows an easy flow of electrons which makes the molecule soft and more reactive,⁵⁶ which means that A4 and B3 compounds are the most reactive in the two series of pyrazine derivatives. For each addition of alkyl-substituted, the energy of the HOMO and LUMO increase respectively but the addition of the fluoro, bromo substituted leads to the decrease of the LUMO energy an exception increase of the bromo substituted and decrease of the fluoro substituted of the HOMO. The carbon C2 has the most important positive charge (0.206) in the compound A4 (2-ethyl pyrazine) for the first series, also for compound B3 (2,3-dibromopyrazine) of the second series, the most important positive charges are on carbon C2 (0.102) and C3 (0.102) as shown in (Table 5), these positions C2 and C3 with the important positive charges lead to preferential sites of nucleophilic attack. The compound B3 is predicted to be the most reactive with a smaller HOMO-LUMO energy gap and with sites of nucleophilic attack, more stable with the maximum value in the heat of formation.

The contour plots of the π like frontier orbital for the ground state of the compound B3 are shown in (Fig. 4).

From the plots, we can observe that the HOMO is a π bonding molecular orbital developed on C5 and C6 atoms, and the LUMO is a π^* anti-bonding molecular orbit-

Table 4. Energies of pyrazine and methyl, ethyl-substituted pyrazine.

		ΔH_f [kcal/mol]	HOMO [au]	LUMO [au]	ΔE [au]	μ [Debye]
A1	Pyrazine	44.09	-0.252	-0.055	0.197	0.00
A2	2-methyl pyrazine	37.05	-0.247	-0.051	0.196	0.59
A3	2,3-di-methyl pyrazine	31.78	-0.243	-0.044	0.199	0.80
A4	2-ethyl pyrazine	30.97	-0.247	-0.051	0.195	0.59
A5	2,3-di-ethyl pyrazine	20.48	-0.242	-0.045	0.196	0.69

Table 5. Energies of pyrazine and fluoro, bromo-substituted pyrazine.

		ΔH_f [kcal/mol]	HOMO [au]	LUMO [au]	ΔE [au]	μ [Debye]
B1	Pyrazine	44.09	-0.253	-0.055	0.197	0.00
B2	2-bromopyrazine	49.73	-0.269	-0.068	0.201	1.50
B3	2,3-dibromopyrazine	55.88	-0.268	-0.075	0.192	2.05
B4	2-fluoro pyrazine	04.15	-0.272	-0.065	0.207	1.33
B5	2,3-di-fluoropyrazine	-33.52	-0.280	-0.069	0.211	2.24

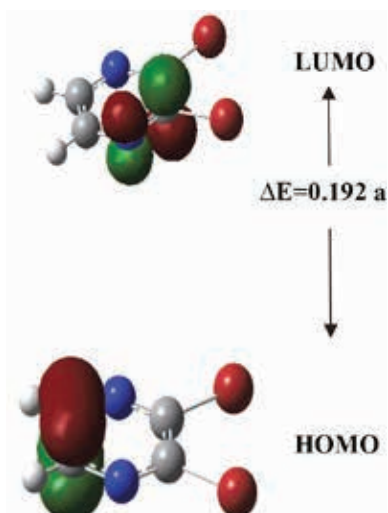
Table 6. NBO charges of pyrazine series 1.

	A1	A2	A3	A4	A5
N1	-0.456	-0.472	-0.471	-0.476	-0.476
N4	-0.456	-0.452	-0.473	-0.452	-0.472
C2	0.013	0.204	0.215	0.206	0.216
C3	0.013	0.016	0.208	0.020	0.213
C5	0.013	0.003	0.010	0.004	0.013
C6	0.013	0.022	0.012	0.023	0.015
C-methyl- 2	-	-0.665	-0.669	-	-
C-methyl- 3	-	-	-0.673	-	-
C ¹ -ethyl- 2	-	-	-	-0.458	-0.459
C ² -ethyl- 2	-	-	-	-0.628	-0.627
C ¹ -ethyl- 3	-	-	-	-	-0.461
C ² -ethyl-3	-	-	-	-	-0.627

Table 7. NBO charges of pyrazine series 2.

	B1	B2	B3	B4	B5
N1	-0.456	-0.458	-0.446	-0.497	-0.485
N4	-0.456	-0.441	-0.446	-0.441	-0.485
C2	0.013	0.112	0.102	0.634	0.586
C3	0.013	0.018	0.102	-0.040	0.586
C5	0.013	0.006	0.018	-0.008	0.002
C6	0.013	0.024	0.018	0.024	0.002
Brome-2	-	0.064	0.100	-	-
Brome-3	-	-	0.100	-	-
Fluor-2	-	-	-	-0.338	-0.327
Fluor-3	-	-	-	-	-0.327

al developed on the N1 and C2 atoms. This further demonstrates the existence of the delocalization of the conjugated π -electron system in 2, 3-dibromopyrazine molecule. Dipole moment equal to zero which confirms the symmetry group D_{2h} of pyrazine. The compound B5 (2, 3-di-fluoropyrazine) also shows a high dipole moment value (2.2435 Debye).

Fig. 4. π like frontier orbitals of the compound B3.

3. 3. Structure Activity/Property Relationship for Pyrazine Derivatives

For the series of pyrazine derivatives (Fig. 8) we have studied seven physicochemical properties with respect to their anti-proliferative activity against the BGC823 (human gastric cell).⁵⁷ The properties involved are: Surface area grid (SAG), molar volume (V), hydration energy (HE), partition coefficient octanol/water (log P), molar refractivity (MR), polarizability (Pol) and molecular weight (MW).

The results obtained using HyperChem 8.0.8 software are shown in Table 8. For example, Fig. 5 shows the favored conformation in 3D of compound 1.

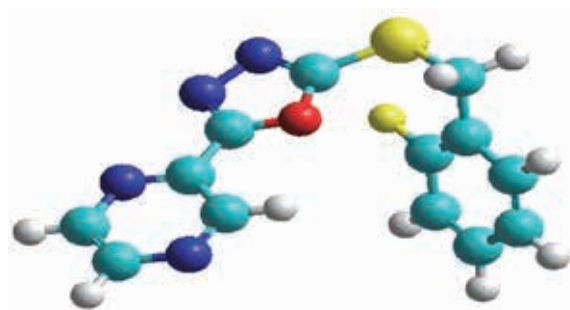


Fig. 5. 3D Conformation of compound 1 (HyperChem 8.03).

Table 8. QSAR properties of pyrazine derivatives.

Compounds	MW [amu]	SAG [Å ²]	V [Å ³]	Pol [Å ³]	MR [Å ³]	LogP	HE [kcal/mol]
1	288.30	466.47	770.17	28.82	79.14	1.94	-12.54
2	304.75	474.61	791.62	30.84	83.73	2.32	-12.63
3	349.20	485.20	810.26	31.54	86.54	2.60	-12.58
4	304.75	498.29	809.75	30.84	83.73	2.32	-13.29
5	349.20	505.96	828.55	31.54	86.54	2.6	-13.24
6	320.81	512.80	828.87	33.20	90.17	2.67	-11.30
7	304.36	486.18	800.84	31.18	85.58	2.29	-11.39
8	320.81	498.70	822.05	33.20	90.17	2.67	-12.25
9	424.32	628.79	1054.66	41.91	118.37	3.13	-11.55
10	363.41	543.20	948.38	39.20	110.97	2.48	-11.54
11	379.87	550.54	984.28	41.21	115.56	2.86	-10.69
12	424.32	554.53	997.06	41.91	118.37	3.13	-10.63
13	379.87	562.49	980.74	41.21	115.56	2.86	-11.45
14	363.41	543.20	948.38	39.20	110.97	2.48	-11.54
15	270.31	475.71	769.23	28.91	79.01	2.55	-13.67
16	286.37	490.32	789.01	31.27	85.45	2.89	-12.89
17	349.20	517.21	832.69	31.54	86.54	2.60	-14.62
18	306.29	476.68	771.74	28.73	79.26	1.34	-13.64

Molar refractivity and polarizability relatively increase with the size and the molecular weight of the studied pyrazine derivatives (Table 8 and fig.6). This result is in agreement with the formula of Lorentz-Lorenz, which gives a relationship between polarizability, molar refractivity and molecular size.

From the obtained results presented in Table 8 and figure 6, we observed that polarizability data and molecular refractivity are generally proportional to the size and the molecular weight of pyrazine derivatives. This explains the congruity of our results with Lorentz-Lorenz expression. For instance, compound 9 and compound 12 show the same maximum values of polarizability (41.91 (Å³)) and refractivity (118.37(Å³)). These compounds have also

high values of molecular weight (424.32 uma), and a slight difference in surfaces and volumes.

Hydration energy in absolute value, the most important is that of the compound 17 (14.62 kcal · mol⁻¹) and the smallest value is that of the compound 12 (10.63 kcal · mol⁻¹). Indeed, in biological environments, the polar molecules are surrounded by water molecules. They have established hydrogen bonds between them.

Hydrophobic groups in pyrazine derivatives induce a decrease of hydration energy.

However, the lipophilie increases proportionally with the hydrophobic features of the substituent. As seen in Table 8, compound 17 is expected to have the highest hydrophilicity, whereas compound number 12 should be

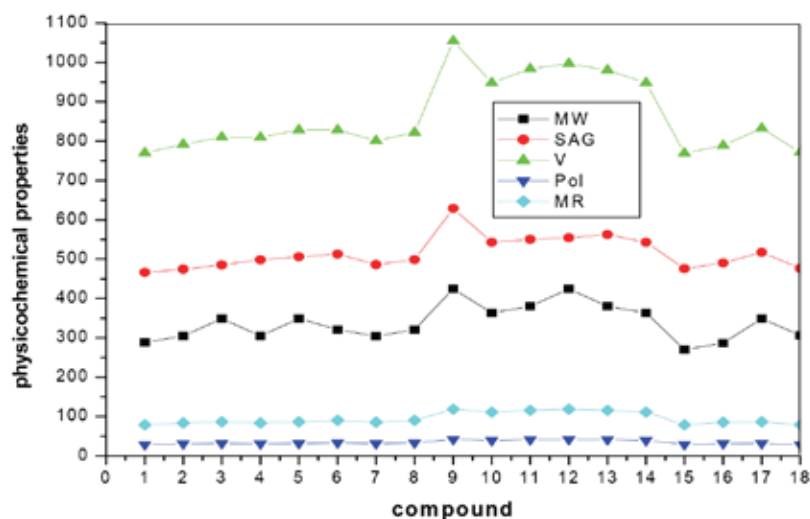


Fig. 6. Graphical representation of physicochemical properties.

most lipophilic. This implies that these compounds should have poor permeability across the cell membrane.

We noticed that compound 17 possess seven hydrogen bond acceptors (HBA) and no hydrogen bond donors (HBD), the presence of hydrophilic groups in this compound result in an increase of the hydration energy. This property explains the ability of these compounds, not only to fix the receptor but also to activate it. Hydration energy measures the degree of agonist character of a potential drug molecule.

Almost ($\log P$) of studied molecules have optimal values. For good oral bioavailability, the $\log P$ must be greater than zero and less than 3 ($0 < \log P < 3$). For very high values of $\log P$, the drug has low solubility and for very low values of $\log P$, the drug has difficulty penetrating the lipid membranes. Thus, compound 17 has the most important hydration energy and the optimal value of $\log P$, the small value of molecular weight leading to better distribution and solubility in fabrics, good oral bioavailability and permeability in cellular membranes respectively (Fig. 7).

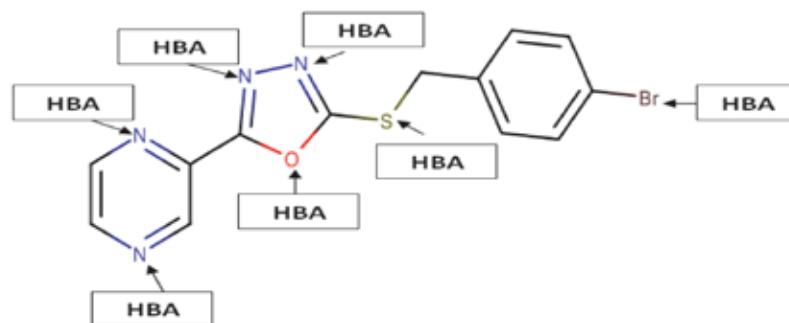


Fig. 7. Acceptor sites of proton for compound 17.

Table 9. Pharmacological activities and properties involved in MPO methods for drug-likeness of pyrazine derivatives.

N°	pIC ₅₀ _{BGC823} ⁵⁷	logP <5	Lipinski's rule			Veber rules	
			MW [amu]	HBA <10	HBD <5	NRB <10	TPSA[A ^{o2}] <140
1	4.74	1.94	288.30	5	0	4	64.71
2	4.56	2.32	304.75	5	0	4	64.71
3	4.76	2.60	349.20	5	0	4	64.71
4	4.8	2.32	304.75	5	0	4	64.71
5	4.94	2.6	349.20	5	0	4	64.71
6	4.87	2.67	320.81	4	0	4	51.57
7	4.73	2.29	304.36	4	0	4	51.57
8	4.69	2.67	320.81	4	0	4	51.57
9	4.70	3.13	424.32	5	0	5	56.50
10	4.53	2.48	363.41	4	0	4	51.57
11	4.46	2.86	379.87	5	0	5	56.50
12	4.44	3.13	424.32	5	0	5	56.50
13	4.69	2.86	379.87	5	0	5	56.50
14	4.57	2.48	363.41	5	0	5	56.50
15	4.60	2.55	270.31	5	0	4	64.71
16	4.67	2.89	286.37	4	0	4	51.57
17	4.59	2.60	349.20	5	0	4	64.71
18	4.48	1.34	306.29	5	0	4	64.71

3. 4. Drug-Likeness Screening Applied in Pyrazine Derivatives

We have applied rules of thumb and calculated metrics of eighteen derivatives of pyrazine (Fig. 8) taken from literature with their anti-proliferative activity against the BGC823.⁵⁷

The properties involved are: octanol/water partition coefficient ($\log P$), molecular weight (MW), hydrogen bond donors (HBD), hydrogen bond acceptors (HBA), number of rotatable bonds (NRB) and polar surface area (TPSA). All the results have been calculated using HyperChem 8.0.8 and Marvin Sketch 6.2.1 software, which are listed respectively in Table 9, we have studied Lipinski and Veber rules to identify “drug-like” compounds:^{58,59}

- (1) There are less than 5 H-bond donors (expressed as the sum of OHs and NHs).
- (2) The molecular weight is under 500 DA.
- (3) The $\log P$ is under 5.
- (4) There are less than 10 H-bond acceptors (expressed as the sum of Ns and Os).

(5) Rotatable bonds are under 10.

(6) TPSA is under 140 \AA^2

All the compounds of the series have the MW under 500 DA, thus they can easily pass through the cell membrane and the better the absorption will be.

There are less than 10 H-bond acceptors and 0 H-bond donors, the fat solubility will be high and therefore the drug will be able to penetrate the cell membrane to reach the inside of the cell. If two of these rules are unsatisfied, the compound will have a problem in absorption and permeability.⁶⁰

TPSA of pyrazine derivatives was found in the range of $52.325\text{--}65.217 \text{ \AA}^2$ and is well below 140 \AA^2 , indicating that these compounds should have good cellular plasmatic membrane permeability. All the screened compounds were flexible, especially; compounds 9 and 11–14 which have 5 rotatable bonds (table 9).

3. 5. Quantitative Structure-Activity Relationships Studies (QSAR) of Pyrazine Derivatives

When chemical or physical properties and molecular structures are derived from numbers, it is often possi-

ble to propose mathematical relations connecting them, which allow making quantitative predictions. The obtained mathematical expressions can then be used as a predictive means of the biological response for similar structures. They are widely used in the pharmaceutical industry to identify promising compounds, especially at the early stages of drug discovery.⁶¹

Relationships between the physicochemical properties of chemical substances and their biological activities can be derived using QSAR (Quantitative Structure-Activity Relationships) concept. These models can also be used to predict the activities of new chemical entities and for their design.⁶² therefore, the biological activity is quantitatively expressed as the concentration of substance necessary to obtain a certain biological response. For that purpose, multiple linear regression, MLR, and artificial neural networks (ANNs) are used. The accuracy of such models is mainly evaluated by the correlation coefficient R^2 .⁶³ The MLR and ANN models were generated using JMP 8.0.2 software.

The equilibrium geometries and the highest occupied molecular orbital energy (E_{HOMO}) and lowest unoccupied molecular orbital energy (E_{LUMO}) and dipole moment (μ) of pyrazine derivatives were determined at the B3LYP/cc-pVDZ level of theory. We list in table 10 of the

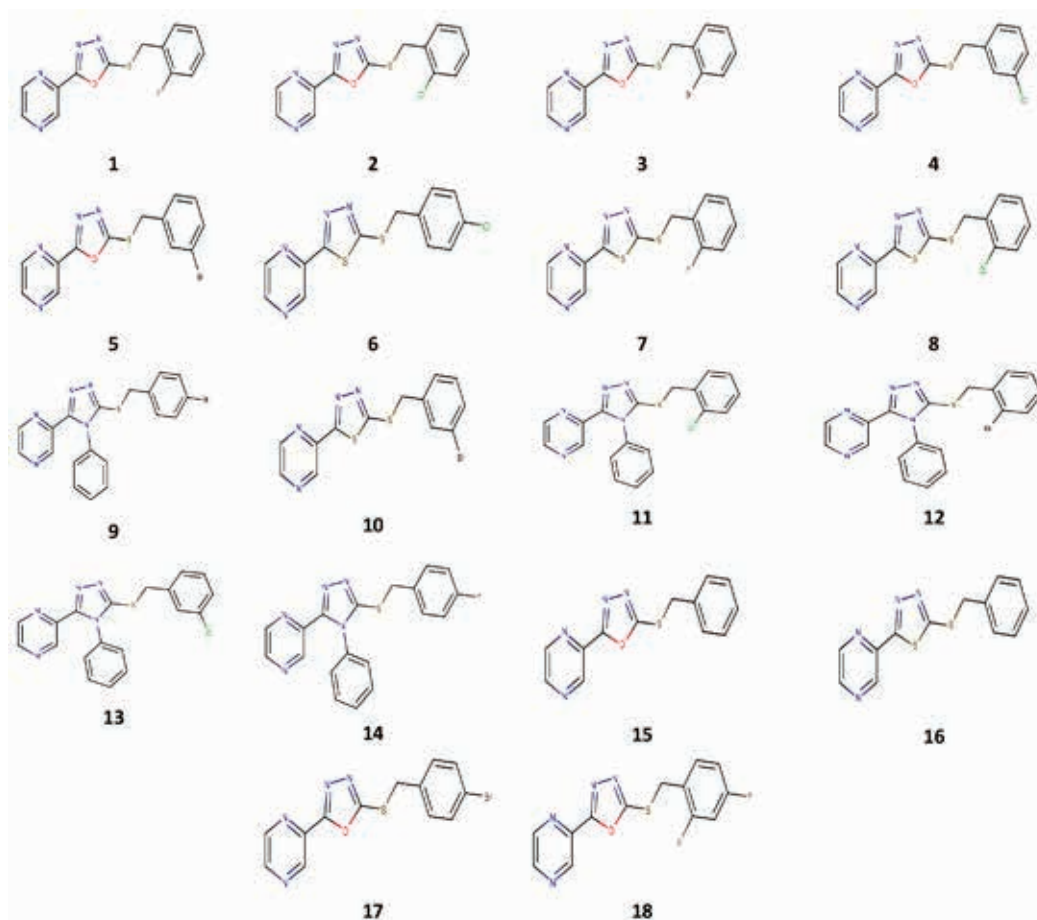


Fig. 8. Structural comparison of pyrazine derivatives.

Table 10. Values of molecular descriptors.

N°	pIC50 _{BGC823} ⁵⁷	V [Å ³]	HE [kcal/mol]	Log P	MR [Å ³]	SAG [Å ²]	MW [amu]	Pol [Å ³]	E _{HOMO} [au]	E _{LUMO} [au]	μ [Debye]
1	4.740	770.170	-12.540	1.940	79.140	466.470	288.300	28.820	-0.239	-0.079	0.886
2	4.560	791.620	-12.630	2.320	83.730	474.610	304.750	30.840	-0.249	-0.081	5.144
3	4.760	810.260	-12.580	2.600	86.540	485.200	349.200	31.540	-0.240	-0.080	0.887
4	4.800	809.750	-13.290	2.320	83.730	498.290	304.750	30.840	-0.243	-0.081	1.269
5	4.940	828.550	-13.240	2.600	86.540	505.960	349.200	31.540	-0.247	-0.082	1.498
6*	4.870	828.870	-11.300	2.670	90.170	512.800	320.810	33.200	-0.236	-0.086	2.564
7	4.730	800.840	-11.390	2.290	85.580	486.180	304.360	31.180	-0.234	-0.084	5.024
8	4.690	822.050	-12.250	2.670	90.170	498.700	320.810	33.200	-0.235	-0.086	5.023
9*	4.700	1054.660	-11.550	3.130	118.370	628.790	424.320	41.910	-0.223	-0.065	4.262
10	4.530	948.380	-11.540	2.480	110.970	543.200	363.410	39.200	-0.223	-0.064	4.275
11*	4.460	984.280	-10.690	2.860	115.560	550.540	379.870	41.210	-0.220	-0.063	4.963
12	4.440	997.060	-10.630	3.130	118.370	554.530	424.320	41.910	-0.220	-0.063	4.949
13	4.690	980.740	-11.450	2.860	115.560	562.490	379.870	41.210	-0.224	-0.067	4.190
14	4.570	948.380	-11.540	2.480	110.970	543.200	363.410	39.200	-0.223	-0.064	4.275
15	4.600	769.230	-13.670	2.550	79.010	475.710	270.310	28.910	-0.240	-0.081	4.278
16	4.670	789.010	-12.890	2.890	85.450	490.320	286.370	31.270	-0.233	-0.083	1.449
17	4.590	832.690	-14.620	2.600	86.540	517.210	349.200	31.540	-0.241	-0.081	4.127
18	4.480	771.740	13.640	1.340	79.260	476.680	306.290	28.730	-0.243	-0.084	4.472

* denotes the selected compounds for external validation (test set).

supplementary material the Cartesian coordinates of the optimized pyrazine derivatives equilibrium structures. Then, the QSAR properties module from Hyper Chem 8.08 was used to calculate: molar weight (MW), surface area (SAG), volume (V), molar refractivity (MR), polarizability (Pol), octanol-water partition coefficient (log P) and hydration energy (HE).

3. 5. 1. Multiple Linear Regression (MLR)

Despite being the oldest, MLR^{64,65} still remains one of the most popular approaches to build QSAR models. This is due to its simple practical use, ease of interpretation and transparency. Indeed, the key algorithm is available and accurate predictions can be provided.⁶⁶ The values of the calculated descriptors are those listed in Table 10. Data were randomly divided into two groups: a training set (internal validation) and a testing set (external validation) at a ratio of 80:20. A correlation matrix between parameters was performed on all nine descriptors. Nevertheless, the analysis revealed six independent descriptors for the development of the model. The significant correlation analysis between biological activity and descriptors is represented by the following equation:

$$\begin{aligned} \text{pIC50}_{\text{BGC823}} = & -6.878 + 0.0115 \\ & \text{V} - 0.0134\text{HE} + 0.1763\text{MR} - 0.0087 \\ & \text{SAG} - 0.004355\text{MAG} - 0.5185\text{Pol} - 15.46 \\ & \text{E}_{\text{HOMO}} - 66.309\text{E}_{\text{LUMO}} - 0.067 \mu \end{aligned} \quad (1)$$

Where, pIC50 is the response or dependent variable (V, HE, MR, SAG, MAG, Pol, E_{HOMO}, E_{LUMO} and μ) are

descriptors (features or independent variables). Within the regression, the coefficients in front of these descriptors are optimized.

The F value (F = 11.84) was found to be statistically significant at 95% level, since all the calculated F value is higher as compared to tabulated values.

For validation of the model, we plot in Fig. 9 the experimental activities against the predicted values as determined by equation (1). We can observe that the predicted pIC50 values are in an acceptable agreement and regular distribution with experimental ones with correlation coefficient (R²) for the training set (R²_{inter} = 0.955) and test set (R²_{ext} = 0.930) indicate the significant correlation between different independent variables with anti-proliferative activity against the BGC823.

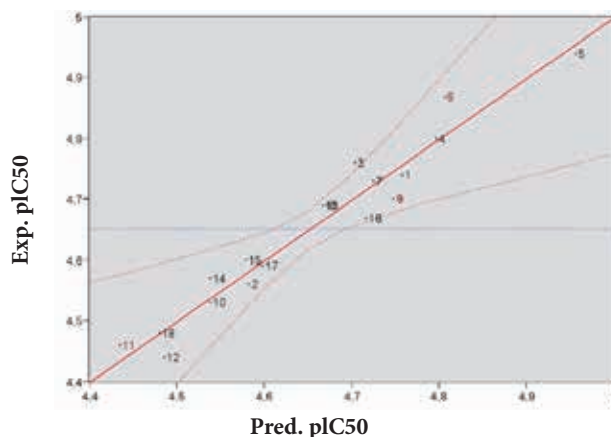


Fig. 9. Correlation of experimental and predicted pIC50 values as derived using MLR.

3. 5. 2. Artificial Neural Networks

ANN^{67–70} is a popular nonlinear model, used to predict the biological activity (i.e. IC₅₀) of the datasets of therapeutic molecules. It presents several benefits like better prediction, adaptation and generalization capacity beyond the studied sample, and better stability of the coefficients. It is employed in complex drug design, drug engineering and medicinal chemistry domains.⁷¹ In this work, the neural network is a system of fully interconnected neurons arranged in three layers. The input layer is made of nine neurons, where each of them receives one of the nine descriptors selected from the correlation matrix of the model. The intermediate (hidden) layer is composed of four neurons that form the deep internal pattern that discovers the most significant correlations between

predicted and experimental data. One neuron constitutes the output layer, which returns the value of pIC₅₀ (Fig. 10).⁷²

As it can be seen in Fig. 10, a good agreement between experimental data and predicted pIC₅₀ issued from the ANN model is observed. Indeed, the statistical parameters for this model, reveal a correlation coefficient close to 1 (= 0.995), indicating that the ANN one is more reliable. Furthermore, the robustness of the model was further confirmed by the significant value of the test data set (= 0.920).

3. 5. 3. Virtual Screening Application

The aim of this study is to identify new structures of pyrazines⁷³ with improved anti-proliferative activity against BGC823 that has to be within the applicability do-

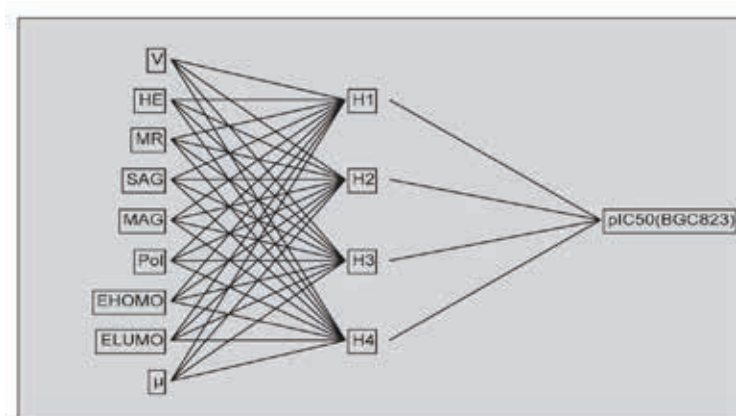


Fig. 10. Structure of ANN.

Table 11. Experimental and predicted pIC₅₀ values using MLR and ANN methods.

N°	Exp. pIC ₅₀ (BGC823)	Pred. pIC ₅₀ (BGC823)	
		MLR	ANN
1	4.740	4.757	4.736
2	4.560	4.582	4.562
3	4.760	4.704	4.764
4	4.800	4.796	4.804
5	4.940	4.956	4.931
6*	4.870	4.806	4.869
7	4.730	4.724	4.717
8	4.690	4.671	4.696
9*	4.700	4.748	4.642
10	4.530	4.537	4.550
11*	4.460	4.434	4.521
12	4.440	4.485	4.443
13	4.690	4.666	4.686
14	4.570	4.537	4.550
15	4.600	4.579	4.603
16	4.670	4.716	4.672
17	4.590	4.598	4.595
18	4.480	4.480	4.481

* denotes the compounds selected for external validation (test set).

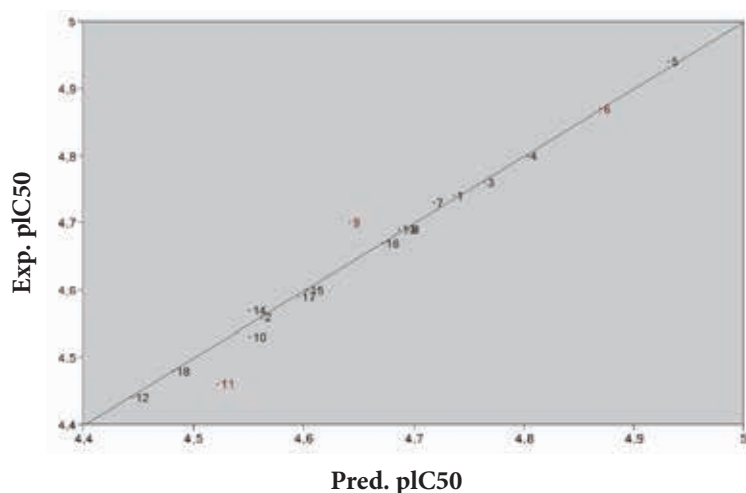
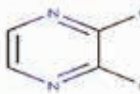
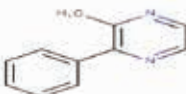
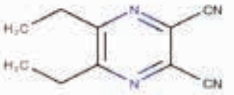
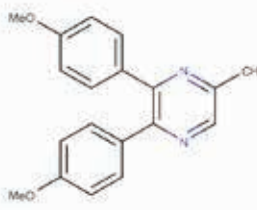
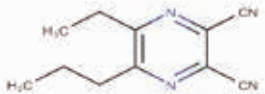
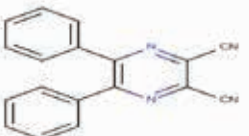
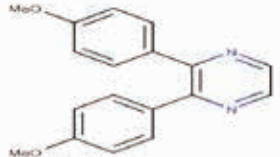
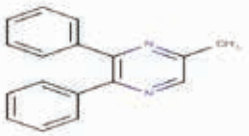
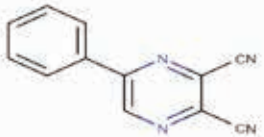
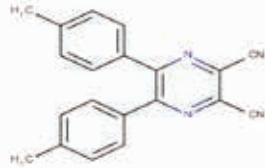
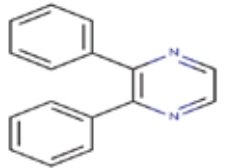
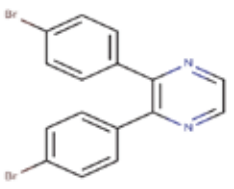


Fig. 11. Correlation of experimental and predicted pIC50 values obtained using ANN.

Table 12. Proposed structural compounds and predicted activities.

No.	Compound structure	pIC50	No.	Compound structure	pIC50
1		6.251	7		2.884
2		5.789	8		3.205
3		4.495	9		7.570
4		2.941	10		3.770
5		6.907	11		7.632
6		3.878	12		4.931

main of the developed model. The structures and activities of these compounds are reported in table 12.

4. Conclusion

The present work deals with the molecular properties of pyrazine. The HF, MP2 and DFT methods, the DFT method is more appropriate for further study on pyrazine rings. The geometry of the pyrazine is symmetric and planar, as all the dihedral angles are either nearly 0° or 180°, which makes this conformation more stable. The compound B3(2,3-dibromo pyrazine) is predicted to be the most reactive with a smaller HOMO–LUMO energy gap of all pyrazine systems, C2 and C3 positions are the most preferential site of nucleophilic attack.

Afterward, we showed that both ANN and MLR methods provide similar QSAR model accuracy. As can be seen in Table 11, the ANN network has substantially better predictive capabilities compared to MLR, leading to pIC50 values closer to the experimental determinations. Nevertheless, both models remain satisfactory and exhibit a high predictive power, thus validating their use to explore and propose new molecules as anti-proliferative activity against the BGC823.

Based on the obtained QSAR equation we have identified a series of potential novel compounds of pyrazine. This series has been used as a primary step for predicting the anti-proliferative activity against the BGC823. It is worth testing the reliability of these predictions in vitro, our work should help in identifying new compounds targeting anti-proliferative activity against the BGC823.

5. References

1. V. M. Baldwin, S. D. Arikatt, T. J. Sindhu, M. Chanran, A. R. Bhat, K. Krishnakumar, *World J. Pharm. Sci.* **2014**, *3*, 1124–1132.
2. D. L. Trump, H. Payne, K. Miller, J. S. de Bono, J. Stephenson, H. Burris, F. Nathan, M. Taboada, T. Morris, A. Hubner, *J. of Prostate*, **2011**, *71*, 1264–1275. DOI:10.1002/pros.21342
3. C. P. Meher, A. M. Rao, Md. Omar, *Asian J. Pharm. Sci. & Res.* **2013**, *3*, 52–56.
4. L. E. Schechter, Q. Lin, D. L. Smith, G. Zhang, Q. Shan, B. Platt, M. R. Brandt, L. A. Dawson, D. Cole, R. Bernotas, A. Robichaud, S. Rosenzweig-Lipson, C.E. Beyer, *Int. J. Neuropsychopharmacol.* **2008**, *33*, 1323–1335. DOI:10.1038/sj.npp.1301503
5. S. Spaia, I. Magoula, G. Tsapas, G. Vayonas, *Perit. Dial. Int.* **2002**, *20*, 47–52. DOI:10.1177/089686080002000109
6. K. Whalen, “*Pharmacology*”, 6th edition, University of Florida, College of Pharmacy Gainesville, Gainesville, Florida, USA, **2014**.
7. S. Rosenzweig-Lipson, J. Zhang, H. Mazandarani, L. H. Boyd, A. sabb, J. Sabalski, G. Stack, G. Welmaker, J. E. Barrett, *J. Dunlop, Brain Res.* **2006**, *1073–1074*, 240–251. DOI:10.1016/j.brainres.2005.12.052
8. W. J. Hehre: Practical Strategies for Electronic Structure Calculations, Wave functions, Irvine, California, USA, **1995**.
9. I. H. Nazli, D. B. Celepci, G. Yakali, D. Topkaya, M. Aygün, S. Alp, *Acta Chim. Slov.* **2018**, *65*, 86–96. DOI:10.17344/acsi.2017.3613
10. F. Odame, *Acta Chim. Slov.* **2018**, *65*, 328–332. DOI:10.17344/acsi.2017.4001
11. S. Belaidi, R. Mazri, H. Belaidi, T. Lanez, D. Bouzidi, *Asian J. Chem.* **2015**, *25*, 9241–9245. DOI:10.14233/ajchem.2013.15199
12. Z. Haddadi, H. Meghezzi, A. Amar, A. Boueckkine, *J. Theor. Comput. Chem.* **2019**, *31*, 595–601. DOI:10.1142/S0219633619500019
13. A. K. Sachan, S. K. Pathak, S. Chand, R. Srivastava, O. Prasad, S. Belaidi, L. Sinha, *Spectrochim. Acta A Mol. Biomol. Spectrosc.* **2014**, *132*, 568–581. DOI:10.1016/j.saa.2014.05.011
14. S. Belaidi, Z. Almi, D. Bouzidi, *J. Comput. Theor. Nanosci.* **2014**, *11*, 2481–2488. DOI:10.1166/jctn.2014.3665
15. C. M. Chang, H. L. Tseng, A. F. Jalbout, A. de Leon, *J. Comput. Theor. Nanosci.* **2013**, *10*, 527–533. DOI:10.1166/jctn.2013.2730
16. T. L. Jensen, J. Moxnes, E. Unneberg, *J. Comput. Theor. Nanosci.* **2013**, *10*, 464–469. DOI:10.1166/jctn.2013.2720
17. M. Ibrahim, H. Elhaes, *Rev. Theor. Sci.* **2013**, *1*, 368–376. DOI:10.1166/rits.2013.1012
18. E. C. Anota, H. H. Cocolletzi, M. Castro, *J. Comput. Theor. Nanosci.* **2013**, *10*, 2542–2546. DOI:10.1166/jctn.2013.3244
19. F. Bazooyar, M. Taherzadeh, C. Niklasson, K. Bolton, *J. Comput. Theor. Nanosci.* **2013**, *10*, 2639–2646. DOI:10.1166/jctn.2013.3263
20. E. R. Davidson : Quantum Theory of Matter, *Chem. Rev.*, guest editor, department of chemistry, Indiana university, India, **1991**, *91*, 649. DOI:10.1021/cr00005a600
21. S. Belaidi, H. Belaidi, D. Bouzidi, *J. Comput. Theor. Nanosci.* **2015**, *12*, 1737–1745. DOI:10.1166/jctn.2015.3952
22. B. Souyei, A. Hadj Seyd, F. Zaiz, A. Rebiai, *Acta Chim. Slov.* **2019**, *66*, 315–325. DOI:10.17344/acsi.2018.4793
23. R. A. Gupta, A. K. Gupta, S. G. Kaskhedikar, *Acta Chim. Slov.* **2009**, *56*, 977–984.
24. E. Zerroug, S. Belaidi, I. Benbrahim, S. Leena, *J. King Saud Univ. Sci.* **2019**, *31*, 595–601. DOI:10.1016/j.jksus.2018.03.024
25. F. Soualmia, S. Belaidi, N. Tchouar, T. Lanez, *J. Fundam. Appl. Sci.* **2020**, *12*, 392–415. DOI: 10.4314/jfas.v12i1S.28.
26. Y. C. Martin: Quantitative Drug Design, Marcel Dekker, New York, USA, **1978**.
27. I. Almi, S. Belaidi, E. Zerroug, M. Alloui, R. G. Ben Said, R. Linguerrri, M. Hochlaf, *J. Mol. Struct.* **2020**, *1211*, 128015. DOI:10.1016/j.molstruc.2020.128015
28. C. A. Lipinski, V. Lombardo, B. W. Dominy, P. J. Feeney, *Adv. Drug Deliv. Rev.* **2001**, *46*, 3–26. DOI:10.1016/S0169-409X(00)00129-0
29. E. L. Pankratov, E. A. Bulaeva, *Rev. Theor. Sci.* **2013**, *1*, 58–82. DOI:10.1166/rits.2013.1004

30. Q. Zhao, *Rev. Theor. Sci.* **2013**, *1*, 83–101.
DOI:10.1166/rits.2013.1005
31. A. Khrennikov, *Rev. Theor. Sci.* **2013**, *1*, 34–57.
DOI:10.1166/rits.2013.1003
32. V. Paitya, K. P. Ghatak, *Rev. Theor. Sci.* **2013**, *1*, 165–305.
DOI:10.1166/rits.2013.1008
33. D. Fisaletti, *Rev. Theor. Sci.* **2013**, *1*, 103–144.
DOI:10.1166/rits.2013.1006
34. D. M. Segall, *J. Curr. Pharm. Des.* **2012**, *18*, 1292–1310.
DOI:10.2174/138161212799436430
35. R. Darnag, B. Minaoui, M. Fakir, *Arab. J. Chem.* **2017**, *10*, 600–608. DOI:10.1016/j.arabjc.2012.10.021
36. P. Xuan, Y. Zhang, T. J. Tzeng, X. F. Wan, F. Luo, *Glycobiology*, **2012**, *22*, 554–560. DOI:10.1093/glycob/cwr163
37. S. Kothiwale, C. Borza, A. Pozzi, J. Meiler, *Molecules*. **2017**, *22*, 1576–1586. DOI:10.3390/molecules22091576
38. Z. Hajimahdi, A. Ranjbar, A. A. Suratgar, A. Zarghi, *Iran. J. Pharm. Res.* **2014**, *14*, 69–74.
39. M. Ghamri, D. Harkati, S. Belaidi, S. Boudergua, R. Ben Said, R. Linguierri, G. Chambaud, M. Hochlaf, *Spectrochim. Acta A Mol. Biomol. Spectrosc.* **2020**, *242*, 118724.
DOI:10.1016/j.saa.2020.118724
40. S. Boudergua, M. Alloui, S. Belaidi, M. Mogren Al Mogren, U. A. Abd Ellatif Ibrahim, M. Hochlaf, *J. Mol. Struct.* **2019**, *1189*, 307–314. DOI:10.1016/j.molstruc.2019.04.004
41. E. Pourbasheer, S. Vahdani, D. Malekzadeh, R. Aalizadeh, A. Ebadi, *Iran. J. Pharm. Res.* **2017**, *16*, 966–980.
42. HyperChem (Molecular Modeling System) Hypercube, Inc., 1115 NW, 4th Street, Gainesville, FL 32601, USA (2008).
43. Gaussian 09, M. J. Frisch, G. W. Trucks, H. B. Schlegel, G. E. Scuseria, M. A. Robb, J. R. Cheeseman, G. Scalmani, V. Barone, B. Mennucci, G. A. Petersson, H. Nakatsuji, M. Caricato, X. Li, H. P. Hratchian, A. F. Izmaylov, J. Bloino, G. Zheng, J. L. Sonnenberg, M. Hada, M. Ehara, K. Toyota, R. Fukuda, J. Hasegawa, M. Ishida, T. Nakajima, Y. Honda, Y. Kitao, H. Nakai, T. Vreven, J. A. Montgomery, J. E. Peralta, F. Ogliaro, M. Bearpark, J. J. Heyd, E. Brothers, K. N. Kudin, V. N. Staroverov, T. Keith, R. Kobayashi, J. Normand, K. Raghavachari, A. Rendell, J. C. Burant, S. S. Iyengar, J. Tomasi, M. Cossi, N. Rega, J. M. Millam, M. Klene, J. E. Knox, J. B. Cross, V. Bakken, C. Adamo, J. Jaramillo, R. Gomperts, R. E. Stratmann, O. Yazyev, A. J. Austin, G. A. Cammi, R. Pomelli, C. Ochterski, J. W. Martin, R. L. Morokuma, K. Zakrzewski, V. G. Voth, P. Salvador, J. J. Dannenberg, S. Dapprich, A. D. Daniels, O. Farkas, J. B. Foresman, J. V. Ortiz, J. Cioslowski, D. J. Fox, Gaussian Inc., Wallingford, CT (2010).
44. MarvinSketch15.8.31, Chemaxon (<http://www.chemaxon.com>) (2015).
45. Database, (<http://www.molinspiration.com>).
46. JMP 8.0.2, SAS Institute Inc., (2009).
47. M. Kanno, Y. Ito, N. Shimakura, S. Koseki, H. Kono, Y. Fujimura, *J. Phys. Chem. - Chem. Phys.* **2015**, *17*, 2012–2024.
DOI:10.1039/C4CP04807E
48. P. Govindasamy, S. Gunasekaran, *J. Mol. Struct.* **2015**, *1081*, 96–109. DOI:10.1016/j.molstruc.2014.10.011
49. J. S. Murray, K. Sen, Molecular Electrostatic Potentials, 1st Edition, Concepts and Applications, Elsevier, Amsterdam, Holland, 1996.
50. I. Alkorta, J. J. Perez, *Int. J. Quantum Chem.* **1996**, *57*, 123–135.
DOI:10.1002/(SICI)1097-461X(1996)57:1<123::AID-QUA14>3.0.CO;2-9
51. E. Scrocco, J. Tomasi, *Adv. Quantum Chem.* **1978**, *11*, 115–193. DOI:10.1016/S0065-3276(08)60236-1
52. F. J. Luque, M. Orozco, P. K. Bhadane, S. R. J. Gadre, *J. Phys. Chem.* **1993**, *97*, 9380–9384. DOI:10.1021/j100139a021
53. J. Sponer, P. Hobza, *J. Quantum Chem.* **1996**, *57*, 959–970.
DOI:10.1002/(SICI)1097-461X(1996)57:5<959::AID-QUA16>3.0.CO;2-S
54. J. M. Seminario, Recent Developments and Applications of Modern Density Functional Theory, Elsevier, Amsterdam, Holland, **1996**. DOI:10.1016/S1380-7323(96)80082-3
55. I. Fleming: Frontier orbitals and organic chemical reactions, Wiley, New York, USA, **1976**.
56. G. L. Miessler, D. A. Tarr: *Inorganic Chemistry*, 2nd edition, Prentice-Hall Upper Saddle River, New Jersey, USA, **1999**.
57. Y. B. Zhang, X. L. Wang, W. Liu, Y. S. Yang, J. F. Tang, H. L. Zhu, *Bioorg. Med. Chem.* **2012**, *20*, 6356–6365. DOI:10.1016/j.bmc.2012.08.059
58. C. A. Lipinski, F. Lombardo, B. W. Dominy, P. J. Feeney, *J. Adv. Drug Deliv. Rev.* **2012**, *64*, 4–17.
DOI:10.1016/j.addr.2012.09.019
59. D. F. Veber, S. R. Johnson, H. Y. Cheng, B. R. Smith, K. W. Ward, K. D. Kopple, *J. Med. Chem.* **2002**, *45*, 2615–2623.
DOI:10.1021/jm020017n
60. M. Aurélien, Ph.D. Dissertation, Orleans University, France, **2006**.
61. F. Soualmia, S. Belaidi, H. Belaidi, N. Tchouar, Z. Almi, *J. Biomed. Sci.* **2017**, *11*, 584–591.
DOI:10.1166/jbns.2017.1476
62. B. Jhanwarb, V. Sharma, R. K. Singla, B. Shrivastava, *Pharmacologyonline*. **2011**, *1*, 306–344.
63. R. Darnag, B. Minaoui, M. Fakir, *Arab. J. Chem.* **2017**, *10*, 600–608. DOI:10.1016/j.arabjc.2012.10.021
64. I. Hammoudan, S. Matchi, M. Bakhouch, S. Belaidi, *Chemistry*, **2021**, *3*(1):391–401. DOI:10.3390/chemistry3010029
65. R. Dahmani, M. Manachou, S. Belaidi, S. Chtita, S. Boughdiri, *New J. Chem.* **2021**, *45*(3), 1253–1262.
DOI:10.1039/D0NJ05298A
66. K. Roy, S. Kar, R. N. Das, A Primer on QSAR/QSPR Modeling: Fundamental Concepts, Springer, New York, USA, **2015**.
67. S. Erić, M. Kalinić, A. Popović, M. Zloh, I. Kuzmanovski, *Int. J. Pharm.* **2012**, *437*, 232–241.
DOI:10.1016/j.ijpharm.2012.08.022
68. R. Lowe, H. Y. Mussa, J. B. Mitchell, R. C. Glen, *J. Chem. Inf. Model.* **2011**, *51*, 1539–1544. DOI:10.1021/ci200128w
69. E. Zerroug, S. Belaidi, S. Chtita, *J. Chin. Chem. Soc.* **2021**, *68*(2), 197–384. DOI:10.1002/jccs.202000457
70. F. Z. Fadel, N. Tchouar, S. Belaidi, F. Soualmia, O. Oukil, and K. Ouadah, *J. Fundam. Appl. Sci.*, **2021**, *13*(2), 942–964.
DOI:10.43 14/jfas.v13i2.17.
71. C. Feng, S. Vijaykumar, *Clin. Exp. Pharmacol.* **2012**, *2*, 2–3.
DOI:10.4172/2161-1459.1000e113

72. B. D. Ripley, Pattern Recognition and Neural Networks, Cambridge University Press, NY United States, USA, 1996.

73. P. Ghosh, A. Mandal, Green Chem. Lett. Rev., 2012, 5(2), 127–134. DOI:10.1080/17518253.2011.585182

Povzetek

Preučevali smo elektronske strukture, vpliv substitucije, povezavo med strukturno fizikalno-kemijskimi lastnostmi ter aktivnostjo in učinkovinske podobnosti (ang. drug-likeness) pirazinskih derivatov s pomočjo *ab initio* (HF, MP2) in B3LYP/DFT (teorijo gostotnega funkcionala). V članku smo izračunali vrednosti naboja NBO (naravnih veznih orbital), dolžino vezi, dipolne momente, elektronsko afiniteto, tvorbeno entalpijo in QSAR lastnosti. Študij QSAR smo izvedli s pomočjo statističnih modelov multiple linearne regresije in nevronske mreže (ANN). Rezultati so pokazali visoko korelacijo med eksperimentalnimi in napovedanimi vrednostmi, s čimer smo preverili in pokazali ustreznost QSAR modelov. Statistična analiza je pokazala, da je ANN z arhitekturo 9-4-1 bolj ustrezna kot MLR. Pregled različnih molekul na osnovi molekularne podobnosti in uporabe QSAR domen je pokazal več kandidatov z izboljšanim antiproliferativnim delovanjem.



Except when otherwise noted, articles in this journal are published under the terms and conditions of the Creative Commons Attribution 4.0 International License